ARTICLE IN PRESS

Available online at www.sciencedirect.com

ScienceDirect

Advances in Space Research xxx (xxxx) xxx

ADVANCES IN SPACE RESEARCH (a COSPAR publication)

www.elsevier.com/locate/asr

CubeSats for space debris removal from LEO: Prototype design of a robotic arm-based deorbiter CubeSat

Sarat Chandra Nagavarapu [a,*], Laveneishyan B. Mogan [b], Amal Chandran [c], Daniel E. Hastings [d]

[a] Institute for Infocomm Research (I2R), Agency for Science, Technology and Research (A*STAR), 138632 Singapore
[b] School of Electrical and Electronic Engineering, Nanyang Technological University (NTU), 639798 Singapore
[c] Laboratory for Atmospheric and Space Physics (LASP), University of Colorado (CU), Boulder, CO 80303, United States
[d] Aeronautics and Astronautics Department, Massachusetts Institute of Technology (MIT), Cambridge, MA 02139, United States

Received 31 January 2024; received in revised form 2 August 2024; accepted 4 August 2024

Abstract

Space debris has become a growing problem, and various studies indicate that the population of space objects has reached a critical density in low Earth orbits (LEO). Therefore, removing debris from the LEO is key to stabilizing the growth of space objects and making some of the orbits reusable for future launches. Deorbiting larger debris objects using miniaturized satellites, CubeSats is both economically viable and requires relatively less time for design & deployment. In this paper, we present a system-level study of orbital debris removal from LEO using CubeSats, detailing various existing debris tracking, rendezvous, capture, and deorbit mechanisms. A deep learning-based object detection algorithm has been utilized to improve the accuracy of detecting and localizing debris. We also present a discussion on the CubeSat-compatible capture & deorbit mechanisms identified from our study and an upper bound on the debris mass that can be deorbited from a given LEO orbit using CubeSats. We aim to demonstrate a case study for the orbital decay analysis of a CubeSat deorbiting the XSat, a microsatellite launched by Singapore. We detail the design of a 27U CubeSat deorbiter prototype equipped with a pair of robotic arms to capture the XSat. This analysis considers active deorbiting using Hall-effect thrusters, for which the required delta-V & propellant mass have also been computed.

Keywords: Space debris; LEO; CubeSat; Satellite; Deorbiter; Robotic arms; Object detection; Capture; Active debris removal; Propellant mass

1. Introduction

Orbital debris has been amassing since the launch of the first satellite into space. Space debris is comprised of both natural and artificial space particles. Natural debris such as meteoroids, comets, etc. are in orbit around the Sun, while most artificial debris is in orbit around the Earth. Thus, man-made debris is more commonly referred to as *orbital debris* (NASA, 2017). Space debris is growing from being a nuisance to becoming a threat to humanity. Operating satellites benefit mankind by making many of our day-to-day activities possible, such as telecommunication, weather forecasting, and localization through global positioning satellite systems used for ground, maritime, and air traffic, remote sensing, etc. However, increased space activity comes at a cost, in terms of the space debris produced,

* Corresponding author.
E-mail address: saratchandra.nagavarapu@gmail.com (S.C. Nagavarapu).

https://doi.org/10.1016/j.asr.2024.08.009
0273-1177/

which makes orbits increasingly overcrowded and poses a serious risk to existing satellites and future space missions. This debris is in the form of derelict satellites, spent upper stages of launchers, fragments resulting from in-orbit collisions and explosions, etc. Operational satellites that are crucial for mankind's infrastructure are threatened by these debris objects traveling at high speeds in space. For satellites operating in LEO, the probability of entering a collision course with other neighboring satellites or debris objects is large. In 1978, the NASA scientist Donald J. Kessler proposed that a cascade of collisions would occur if the concentration of orbital debris becomes dense enough, even if all launches into space would be stopped immediately (Liou, 2006; Shan et al., 2016). This theoretical scenario is referred to as *Kessler Syndrome*. Each collision would generate more debris, amplifying the risk of future break-ups and exacerbating the problem (Liou, 2018).

The January 11, 2007 event where China destroyed its Fengyun-1C weather satellite with a ground-based missile resulted in over 100,000 pieces of debris, including 950 larger than 4 inches (Kan, 2007). The collision between Iridium 33 and Cosmos 2251 on February 10, 2009, produced around 5,000 large debris pieces, posing significant threats to 500 operational satellites nearby (Liou and Shoots, 2009). In 2019, ESA maneuvered one of its Earth science satellites to avoid a collision with a SpaceX Starlink satellite (ESA, 2019). The rise of satellite mega-constellations like Starlink is expected to double space traffic over the next decade, leading to more frequent close approaches and collisions, thereby increasing debris density in LEO (Witze, 2019).

As of December 2023, over 130 million pieces of debris ranging from 1 mm to 1 cm, approximately 1 million pieces from 1 cm to 10 cm, and around 36,500 larger than 10 cm were estimated to orbit Earth (ESA, 2023). Additionally, fragments resulting from collisions, though tiny, pose safety concerns for human space missions in LEO (Liou and Johnson, 2006). Therefore, space debris removal is crucial. Adhering to the 25-year safety lifetime standard for satellites below 2000 km altitude is thus crucial (Liou, 2014). Enforcing this rule is vital, as NASA predicts the need to remove 5 to 10 space debris objects annually to stabilize the space environment (ESA, 2016). Jamie Morin advocates a global space traffic management strategy focusing on tracking, prediction, identification, standards, norms, and debris reduction (Morin, 2019).

Space debris can arise from various sources, including hypervelocity impacts with orbiting spacecraft, explosions (both high and low intensity), decommissioned satellites, and leftover rocket upper stages. Since 1975, NASA has been monitoring the mass distribution of space debris in LEO. Analysis reveals that orbits near 800 km altitude are particularly congested (Liou et al., 2010), with higher densities of debris observed at altitudes of 600 km, 800 km, and 1000 km. These regions harbor the majority of debris weighing over 50 kg, as depicted in Fig. 1.

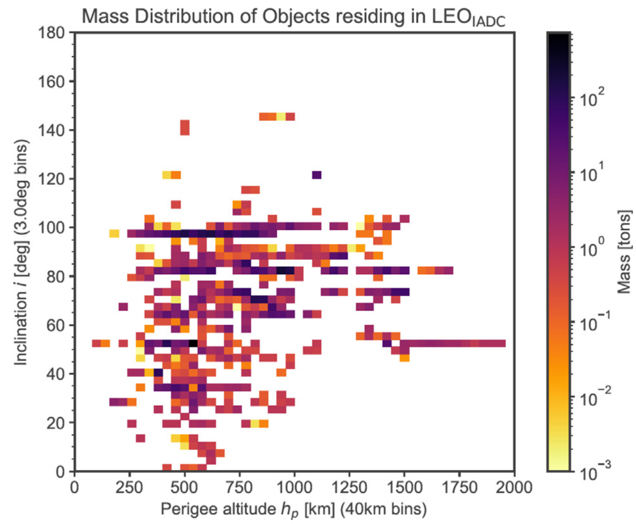

Fig. 1. Mass distribution of objects in LEO (ESOC, 2023).

Recent years have witnessed a surge in research on space debris removal, garnering interest from academia and industry. Leading companies like Astroscale offer End of Life (EOL) and Active Debris Removal (ADR) services, exemplified by successful in-orbit demonstrations such as the ELSA-d satellite missions in 2021 (Astroscale, 2019). Similarly, the Swiss start-up *The CleanSpace One*, in collaboration with ESA, develops debris removal satellites equipped with nets and robotic arms to clear medium and large-size debris from LEO (CleanSpaceOne, 2019). These efforts are vital for sustaining future space activities, particularly in orbits below 1000 km. Moreover, leveraging small satellites, notably CubeSats, presents a cost-effective and scalable approach to debris removal, enhancing the feasibility of such endeavors from both commercial and economic perspectives.

The paper is structured as follows: Section 2 outlines the debris removal process and existing techniques for tracking, rendezvous, capture, and deorbit. Section 3 explores the use of CubeSats for debris removal and compatible capture mechanisms. Section 4 covers drag equations, the NRLMSISE-00 atmospheric model, and factors influencing orbital decay, along with upper limits on debris mass deorbitable using CubeSats. Section 5 presents a case study on the XSat deorbit mission, detailing the deorbiter CubeSat prototype design with several subsystems, dual robotic arm-based debris capture device, an object detection and tracking algorithm using deep learning framework, various deorbit mechanisms, and delta-V and propellant mass computation for active deorbiting, and orbital decay analysis. Section 6 offers a discussion on the practicality of CubeSat-based debris removal, including insights into form factor selection. Finally, conclusions are drawn in Section 7.

2. Space debris removal

In a September 2023 ESA report on space debris, it was found that out of 11,500 satellites orbiting the Earth, approximately 9,000 are still operational, leaving over 2,500 inactive satellites that contribute to collision risks and orbital congestion (ESA, 2023). Additionally, Space Surveillance Networks (SSN) track around 35,150 debris objects, with a total estimated mass of over 11,500 tonnes. This rapid growth of space debris presents a significant and pressing challenge that requires careful attention. Fig. 2 illustrates the projected growth of debris in low, medium, and geostationary Earth orbits over the next 200 years if no debris removal efforts are undertaken despite halting all space missions.

The estimated number of explosions, collisions, breakups, or unanticipated events resulting in fragmentation is more than 550 (ESA, 2023). As humans launch more and more objects, these numbers are further going up and turning Earth's orbits into a dangerous and crowded junkyard. Therefore, removing or burning up this debris by deorbiting it is an essential task to facilitate future space missions.

The next section presents details on debris removal procedure, and existing techniques for debris capture and deorbit.

2.1. Debris removal - overall picture

Debris removal has been one of the important topics in space research for the last decade. A space mission for debris removal consists of the following phases: launch and commissioning, tracking, far/close-range rendezvous phase, capturing phase, and deorbit phase. These phases can be performed either autonomously or remotely controlled by ground-based mission operations. Out of the five steps involved in the debris removal procedure, as shown in Fig. 3, the capture phase plays a crucial role in the entire mission. However, achieving cost-effective debris removal poses numerous challenges in technology, system engineering, policy, and operations.

A comprehensive review of existing debris removal methods can be found in several sources (Mark and Kamath, 2019; Hakima and Emami, 2018; Bonnal et al., 2013; Shan et al., 2016). Additionally, policy design issues arise, as a debris removal system may impact other space systems where operators or owners may not consent to

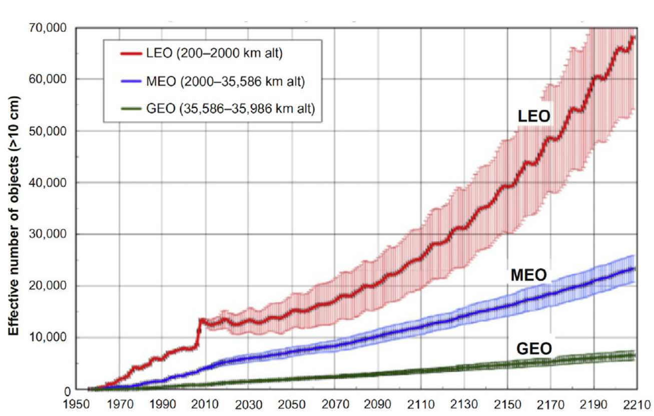

Fig. 2. Estimated space debris growth around the Earth (Liou, 2013).

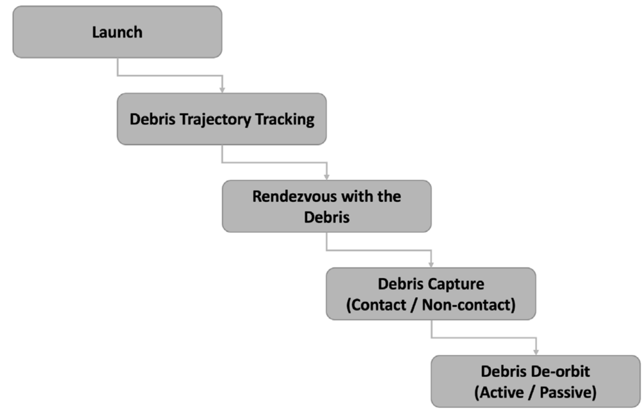

Fig. 3. Space debris removal - Procedure.

its movement. Moreover, any debris removal system must adhere to a version of the Hippocratic oath, *First, do no harm,* ensuring that it does not create new debris.

The next section focuses on the investigation of existing debris tracking, rendezvous, capture, and deorbit mechanisms, assuming the satellite launch is handled without any failure.

2.2. Debris tracking and rendezvous mechanisms

Capturing space debris requires precise tracking and maneuvering of the satellite housing the capturing device near the target debris through rendezvous procedures. Object tracking involves identifying and estimating the trajectory of the target object using radar, cameras, or optical detectors like LiDAR. Vision-based systems offer advantages such as low power consumption, cost-effectiveness, and accurate positioning. Data from these devices, including range and orientation information, are processed via optimization algorithms to predict the target trajectory. Once the target object is located, the capturing satellite employs active propulsion, such as thrusters or jets, to approach it, a process known as rendezvous in 3D space. Various debris tracking and rendezvous approaches using different sensing instruments are documented in the literature.

Vision-based satellite tracking is a cutting-edge method for monitoring space debris. The RemoveDebris project (Forshaw et al., 2020; Aglietti et al., 2020) showcases this with its highly advanced tracking and navigation system. LiDAR-derived point cloud data is processed alongside depth camera data to accurately determine the distance to the debris object. An onboard camera extracts feature points from the object to estimate its orientation. A prediction algorithm continuously monitors the target's trajectory and tumbling. Periodic use of an RGB camera helps reduce computation errors.

Estimating a target's attitude from a distance in space is challenging, emphasizing the need for precise rendezvous during capture or docking. Active propulsion methods like cold gas thrusters, resistojets, and Hall-effect thrusters

(HET) maneuver the chaser satellite around the target, minimizing collision risks and ensuring accurate trajectory alignment (Yamamoto et al., 2014). Two primary rendezvous methods are utilized: the linear approach, moving directly towards the target for docking scenarios like the ISS; and the spiral approach, orbiting the target in a decreasing spiral for accurate line-of-sight and reduced collision risks, particularly preferred for debris capture.

Rendezvous for spacecraft proximity operations has been extensively studied in the literature. Barbee et al. proposed a series method to identify feasible rendezvous sequences with low computational load (Barbee et al., 2011). Braun et al. used a brute-force approach to explore fixed-length rendezvous sequences, estimating mission costs for various scenarios (Braun et al., 2013). Cerf developed a three-step transfer strategy based on RAAN drift and created a rendezvous cost model using the response surface method (Cerf, 2015). Yu et al. employed a hybrid optimal control framework to tackle different variable types in optimal ADR scheduling problems, utilizing simulated annealing for multi-target missions (Yu et al., 2015). Additionally, Bérend and Olive addressed the ADR problem as a time-dependent TSP, applying ant colony optimization, while Shen et al. used the branch-and-bound algorithm to investigate optimal rendezvous sequences (Bérend and Olive, 2016; Shen et al., 2018).

2.3. Debris capture mechanisms

Space debris capture mechanisms fall into two main categories: contact and contactless techniques. Contact capture involves the capturing satellite attaching itself cooperatively to the debris object, then using onboard propulsion to deorbit it. Methods include space nets, sticky booms, harpoons, and robotic arms/grippers/tentacles.

The debris capture mechanism using space nets (Shan et al., 2017) involves launching a large net at the target debris, allowing the chaser satellite to remain at a safe distance. This method is flexible, lightweight, cost-efficient, and CubeSat-compatible (Shan et al., 2017). The RemoveDebris project (Forshaw et al., 2020; Aglietti et al., 2020), a collaboration between Surrey Space Center and Airbus, successfully tested a harpoon device on a dummy target. The harpoon, equipped with barbs, can penetrate large debris objects, accommodating various shapes and maintaining a standoff distance. However, it may create new debris upon impact if fragmentation occurs.

To capture non-cooperative debris like tumbling rocket upper stages, a robust robot manipulator with thruster-controlled joints has been developed (Felicetti et al., 2016). A tentacled robot concept, featuring tentacle arms on a chaser spacecraft, has also been proposed for capturing and detumbling non-cooperative targets (Wilde et al., 2017; Feng et al., 2017). Additionally, a brush-type contactor has been explored as an end-effector for reducing the rotational rate of tumbling debris using a joint virtual depth control algorithm (Nishida and Kawamoto, 2011). Altius Space Machines has developed the *sticky boom*, a boom system with an electro-adhesion pad at its tip for space debris capture (MITTechnologyReview, 2011). This device extends up to 100 meters and uses electro-adhesion to securely attach to target objects, regardless of their original design for grappling.

The Sling-Sat Space Sweeper (4S), developed by Texas A&M University, is a contact-type debris removal mechanism (Missel and Mortari, 2013). It features a dual-arm design with a tri-scissor structure that adjusts arm length to capture and eject multiple debris objects from LEO. Another contact-based capture method involves using dry/wet adhesives, effective for small and medium-sized debris in LEO. Controlled dry adhesion (CDA), or gecko-inspired adhesives, has proven effective for capturing space debris (Bylard et al., 2017; Trentlage and Stoll, 2015). CDA is cost-effective, resilient to radiation, vacuum conditions, and extreme temperatures, and allows for attachment and detachment with minimal force, reducing the risk of generating additional debris.

Techniques such as electro-static tractors, gravity tractors, etc. fall under the category of contactless capture, where no physical connection is made between the chaser and the target debris. Instead, they utilize the chaser's gravitational or electrostatic force fields to transmit the necessary impulse for capturing or repelling the target debris from its orbit. Table 1 outlines various methods for capturing space debris based on the target debris size, as documented in the literature.

2.4. Debris deorbit mechanisms

Once the chaser satellite has successfully captured the tracked space debris, the subsequent objective is to deorbit the debris by directing it towards Earth to disintegrate during reentry. Phipps et al. proposed the Laser Orbital Debris Removal (LODR) technique, using a high-power pulsed laser system from Earth to generate plasma jets on debris, decelerating them for atmospheric incineration (Phipps and Bonnal, 2016). Recently, SKY Perfect JSAT Corporation, in collaboration with Japanese research institutions including JAXA, announced a 2026 debris removal mission focused on developing a laser-equipped satellite for debris removal (Kyushu, 2020).

Utilizing gas or plasma to eject space debris is another innovative solution. Takahashi et al. demonstrated the effectiveness of bi-directional plasma ejection via an open exit magnetic nozzle RF plasma thruster, which imparts force to debris while maintaining zero net thrust on the thruster (Takahashi et al., 2018). For heavier debris, such as rocket upper stages exceeding 500 kg, a hybrid propulsion-based rocket system has been developed. This system, described in (DeLuca et al., 2013), involves transferring the engine from a servicing platform to the debris via a robotic arm for controlled disposal.

Increasing the surface area of space debris enhances atmospheric drag, facilitating re-entry and disposal. Drag

Table 1
Debris capture mechanisms for various debris sizes.

	Small	Medium	Large
Harpoons	–	–	✓
Space Adhesives	✓	✓	–
Sticky Booms	–	✓	✓
Space Nets	–	✓	✓
Robotic Arms or Tentacles	–	✓	✓

augmentation methods involve attaching gossamer structures, space balloons, or drag/solar sails to debris, lowering orbit altitude and enabling atmospheric re-entry and combustion. Chandra et al. proposed a structural design for an inflatable gossamer aero-braking device to de-orbit small satellites (Chandra et al., 2019), featuring an inflatable sphere and toroid with aero-brake capabilities.

The GOLD (Gossamer Orbit Lowering Device) is an inflatable membrane designed to increase the drag surface area of space debris, facilitating faster reentry (Nock et al., 2010). Similar devices, like the deorbiting gossamer, reduce debris's ballistic coefficient to achieve disposal (Fernandez et al., 2013). Solar sails leverage solar radiation momentum to propel spacecraft (Romagnoli and Theil, 2012), and CubeSail, a CubeSat-compatible drag sail system, is tailored for de-orbiting smaller spacecraft or debris from LEO (Lappas et al., 2011). Table 2 outlines various space debris deorbit techniques found in the literature.

The next section details the CubeSat satellite system and the advantages of deploying these for debris removal.

3. CubeSats for space debris removal

The economic viability, ease of satellite design, and affordable loss are among the major concerns in deploying a satellite system for space debris removal. These factors have led to the preference for small satellites, typically under 500 kg, as a feasible option. The emergence of CubeSats, enabled by advancements in electronics, has further facilitated satellite development. CubeSats offer cost-effectiveness, shorter development times, smaller form factors, and ease of launch. Their reduced size also translates to lower launch costs, as they can share a rocket with larger satellites, maximizing space utilization. As a result, the space research community is increasingly focusing on developing and deploying CubeSats for debris removal.

Table 2
Debris deorbit mechanisms for various debris sizes.

	Small	Medium	Large
Sails (Drag/Solar/Magnetic)	–	✓	✓
Ion Beam Shepherd	–	✓	✓
Space Balloons	–	–	✓
Giant Space Lasers	–	-	✓
Gossamers	–	✓	✓

CubeSats, miniature satellites extensively used in LEO over the past two decades, were first proposed in 1999 by Jordi Puig-Suari of California Polytechnic State University and Bob Twiggs of Stanford University. Originally intended as training tools for students to learn about flight hardware design, construction, testing, and operations, CubeSats are built to standard dimensions of 10 cm × 10 cm × 10 cm, known as one unit (1U) (CalPoly, 2014). They can be configured in sizes such as 1U, 3U, 6U, 9U, or 27U, typically weighing less than 1.33 kg (3 lbs) per unit. CubeSats often use commercial off-the-shelf components for their electronics and structural designs. Advancements in miniaturization and the use of these components have made CubeSats cost-effective platforms suitable for specialized tasks. Despite their size and functional limitations, their compact form factor and low mass make them an attractive option for future space missions. Fig. 4 shows the form factor of the InspireSat-1, InspireSat-2, InspireSat-3, and InspireSat-4 (ARCADE) satellites.

CubeSats are increasingly prominent in debris removal missions due to their compact design and ease of assembly using off-the-shelf electronic components. Lucken et al. propose a constellation of 6U CubeSats equipped with stereoscopic detection systems, integrated LIDAR, and ion thrusters for tracking and removing debris (Lucken et al., 2017). Another mission described in (Hakima et al., 2018) involves deploying a CubeSat from a mothership to capture and stabilize target debris before reentry. Additionally, a deployable drag deorbit device (D3) with retractable tape spring booms is designed to fit inside a 12U CubeSat for orbital maneuvering and collision avoidance (Guglielmo et al., 2019).

3.1. CubeSat compatible debris capture and deobrit techniques

We have also identified various debris capture and deorbit techniques that a CubeSat-based system could potentially use to remove debris multiple times from LEO during its lifespan. Considering the dimensions and mass of the existing debris capture and deorbit devices, we have listed their compatibility with the 27U, 9U, and 6U CubeSat form factors. Table 3 presents these CubeSat-compatible debris capture and deorbit methods for various satellite form factors.

An appropriate combination of debris capture and deorbit mechanisms can be chosen to come up with a miniature satellite system for debris removal within an allowable CubeSat form factor size.

4. Debris orbital lifetime analysis

To remove debris from densely populated orbits, it is recommended that satellites and orbital stages be commanded to reenter Earth's atmosphere within 25 years of mission completion if their deployment orbit altitude is below 2000 km (in the LEO region) (Liou, 2014). For inac-

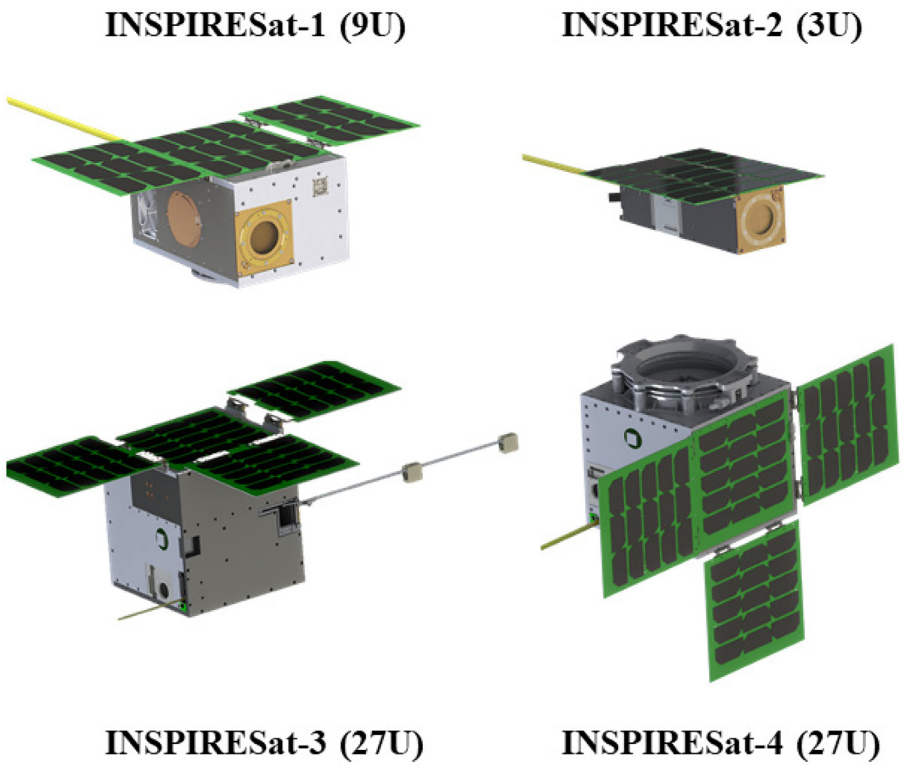

Fig. 4. The INSPIRESat-1, INSPIRESat-2, INSPIRESat-3 and INSPIRESat-4 satellites.

tive satellites and upper stages in or near the geostationary ring, raising their orbits to a graveyard orbit, which is about 300 km above the GEO ring, is the only viable option. The lifetime or orbital decay or the Earth re-entry time of space debris depends on three major parameters, namely solar radiation flux measured by F10.7 cm, and the drag surface area. Therefore, for a satellite commissioned to deorbit space debris, these parameters, in turn, define its lifetime during reentry.

The decay of satellites in low Earth orbit (LEO) is influenced by the drag force they experience from interactions with the sparse atmosphere and up-flow from the Earth. At LEO altitudes, atmospheric density is primarily controlled by solar flux and particle precipitation from the magnetosphere. This decay determines the physical lifetimes of satellites, making lifetime prediction crucial for space research, tracking, and mission planning. Predicting lifetimes relies on initial orbital parameters, satellite mass-to-area ratio, and atmospheric density variations. Despite atmospheric models, uncertainties persist due to factors like satellite attitude and solar/geomagnetic indices.

The subsequent sections provide comprehensive explanations of the drag and orbital period decay equations, the MSISE atmospheric density model, and the influence of drag surface area on orbital decay.

Table 3
CubeSat compatible debris capture and deorbit mechanisms w.r.t. CubeSat size.

	6U	9U	27U
Debris Capture Mechanisms			
Harpoons	–	✓	✓
Space Adhesives	–	✓	✓
Sticky Booms	–	✓	✓
Robotic Arms/Grippers/Tentacles	–	✓	✓
Space Nets	–	–	✓
Debris Deorbit Mechanisms			
Sails (Drag/Solar/Magnetic)	✓	✓	✓
Space Balloons	✓	✓	✓
Gossamers	✓	✓	✓

4.1. Drag and orbital decay computations

Atmospheric drag is the frictional force exerted by the atmosphere acting opposite to the relative motion of an object (Gaposchkin and Coster, 1988). When a spacecraft travels through the atmosphere, it experiences a drag force in a direction opposite to the direction of its motion. The expression for the drag force is as follows:

$$D = \frac{1}{2}\rho v^2 A C_d. \quad (1)$$

Here D is the drag force, ρ is the atmospheric density, v is the velocity of the satellite relative to the atmosphere, A is its cross-sectional area perpendicular to the direction of motion, and C_d is the surface drag coefficient. By substituting this drag force in Newton's second law together with orbital energy equations, we can derive an expression for the change in the orbital period of the satellite with time as

$$\Delta P = -3\pi h \rho (A C_d / m_s) \Delta t. \quad (2)$$

Here P is the orbital period, h is the semi-major axis, Δt is the time step increment used for the simulation, and m_s is the mass of the satellite respectively.

4.2. Upper limit on debris mass for cubesats in LEO

To regulate space operations, all space organizations & industries are directed to follow the 25-year safety lifetime standard for spacecraft, which states that all the satellites that are functional in LEO, should lower their orbit and reenter the Earth's atmosphere within 25 years of mission completion (Liou, 2014). From Eq. 2, the orbital period decrement equation, the CubeSat's lifetime depends on its orbit altitude h, drag surface area A, atmospheric density ρ, and the total mass of the satellite, denoted as m_t, is the sum of the satellite mass m_s and the debris mass m_d. It is also clear that, if the total mass of the satellite m_t increases, the decay in the orbital period decreases, which results in a longer orbital lifetime. For all the remaining parameters, it is a proportional variation with the orbital period decay.

Therefore, to adhere to the 25-year post-mission orbit time rule, using Eq. 2, we have computed the upper bound on the total debris mass (m_t) that can be deorbited for a given C_d, A, h and ρ, assuming the only force is the drag force. Despite the mechanical & technical challenges that are associated with debris capture, this limit corresponds to the maximum possible debris mass that can be deorbited from a given altitude in LEO using a CubeSat under the effect of all other parameters. Fig. 5 illustrates the debris mass upper limits computed for a 27U CubeSat deorbiting from various altitudes in LEO without any sail, with 1 m^2 and 4 m^2 drag sails.

4.3. The NRLMSISE-00 Model

NRLMSISE-00 is an empirical, global reference atmospheric model (Picone et al., 2002) of the Earth from ground to space. It models the temperatures and densities of the atmosphere's components. NRL stands for the US Naval Research Laboratory. MSIS stands for mass spectrometer and incoherent scatter radar, the two primary data sources for the development of earlier versions of the model. E indicates that the model extends from the ground through the exosphere and 00 is the year of release, which is 2000.

The MSISE00 empirical atmosphere model was developed by Mike Picone, Alan Hedin, and Doug Drob based on the MSISE90 model. The main differences to MSISE90 involve the extensive use of drag and accelerometer data on total mass density, the addition of a component to the total mass density that accounts for possibly significant contributions of O+ and hot oxygen at altitudes above 500 km, and the inclusion of the SMM UV occultation data on O_2. A primary use of this model is to aid predictions of satellite orbital decay due to atmospheric drag. The MSISE model describes the neutral temperature and densities in Earth's atmosphere from ground to thermospheric heights.

4.4. Solar flux and drag surface area & their effect on orbital decay

The Sun's magnetic field undergoes a cyclic variation known as the solar cycle, providing predictability to solar activity. Among environmental factors, the F10.7 index, derived from solar radio flux measurements at 10.7 cm, is a key indicator of solar activity, influencing orbital decay significantly (Tapping, 2013). Originating from the solar chromosphere and corona, F10.7 correlates with sunspot numbers and various solar irradiance records, aiding in space weather specification and forecasting (NOAA, 2020).

The drag cross-sectional area is one of the key parameters, which has a drastic effect on the satellite's lifetime. From Eq. 1, increasing this area enhances the drag force and reduces the orbital lifetime. Various passive deorbiting devices like space balloons, sails, drag nets, terminator tapes, deployable booms, exo-brake parachute systems, etc. exploit this principle, economically aiding satellite reentry. Despite their effectiveness, these systems may face challenges like instability, increased collision risks, punctures, etc. Nonetheless, they remain valuable for meeting the 25-year lifetime requirements in lower orbits.

The next section presents a case study for the XSat deorbit mission using a CubeSat.

5. XSat deorbit mission using a cubesat: a case study

XSat is a microsatellite technology demonstration mission of CREST (Centre for Research in Satellite Technologies), a joint venture of NTU (Nanyang Technology University), and DSO (Defence Science Organization) National Laboratories, Singapore (EOPortal, 2016). XSat was Singapore's first indigenously built satellite at the Satellite Research Centre (SaRC), NTU. The overall objective is to demonstrate technology in support of high-resolution imaging capabilities and to analyze and implement onboard parallel processing algorithms, thereby

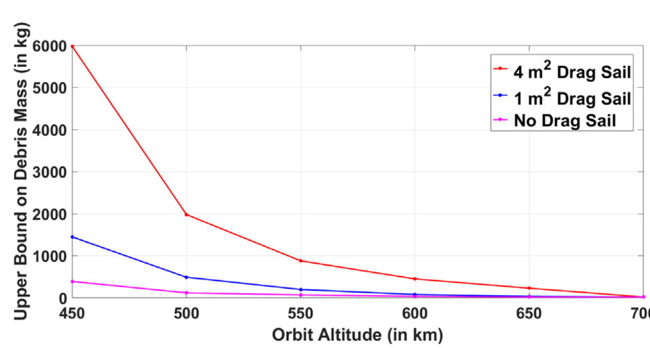

Fig. 5. Upper bound on debris mass for 27U CubeSats deorbiting with debris from various altitudes in LEO with/without a drag sail.

demonstrating improved mission achievements for generally downlink-limited small satellite imaging missions. The XSat was launched on April 20, 2011, in a Sun-synchronous circular orbit at 817 km, with a 98.73-degree inclination. Fig. 6 shows the XSat satellite in the stowed configuration.

The bus structure of the XSat has dimensions of 600 mm × 600 mm × 800 mm and a total mass of 106 kg (EOPortal, 2016). The box design is made of a honeycomb panel structure, which carries the individual components mounted on the respective panels. In addition to the six body panels, a central shelf is provided. XSat employs a tray structure: there are up to 16 stacked trays with different electronics mounted inside.

In this case study, we provide detailed information at the subsystem level for a prototype deorbiter CubeSat that we designed. Additionally, we analyze the orbital decay dynamics associated with the deorbiting of a CubeSat in conjunction with the XSat. XSat has completed its operational objective and, while still beaconing, is nearing its end of life and expected to be decommissioned this year. The following sections emphasize the deorbiter CubeSat design, dual robotic arm-based debris capture subsystem, and two different debris removal subsystems for the XSat deorbit mission, effects of the variation in solar flux F10.7 cm and drag surface area on the satellite lifetime. Throughout this paper, the term *satellite lifetime* refers to the lifetime of the satellite deorbiting with the captured debris object, i.e. the XSat.

5.1. XSat deorbiter cubesat: prototype design & subsystems

In this section, we introduce the design of the XSat deorbiter CubeSat, incorporating debris tracking, rendezvous, capture, and deorbit subsystems alongside standard CubeSat components like antennas, transponders, CDH, ADCS, EPS, thermal control, housing, and solar panels. Fig. 7 illustrates the 3D model of the debris deorbiter CubeSat. For the XSat deorbit mission, a vision-based navigation system is selected for target tracking, offering accuracy and low power consumption. Two Hall-effect thrusters with a specific impulse of 800 s and a power requirement of 50 W, capable of producing peak thrust at 1.5 mN, are chosen for rendezvous and active deorbiting. A dual robotic arm-based capture device is designed to avoid generating additional debris and ensure a secure grip during the deorbit phase. For passive deorbiting, a compact drag sail is adopted, with most devices fitting within a 2U-sized container if their cross-sectional area is less than 4 m^2.

Consolidating all the chosen subsystem sizes, the resultant overall form factor of the deorbiter CubeSat would be 27U. Table 4 illustrates the size of each subsystem in the CubeSat. As the rendezvous phase utilizes the onboard computer to run the optimization algorithms and the Hall-effect thrusters to perform proximity maneuvers, it does

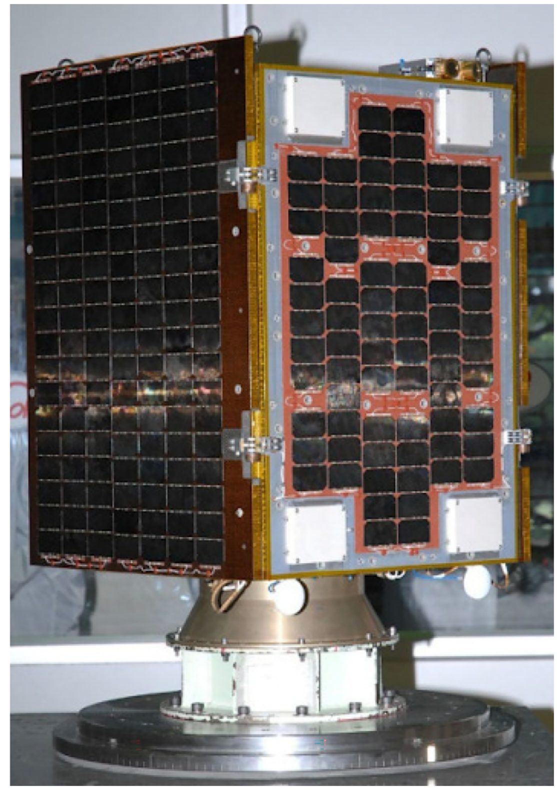

Fig. 6. The XSat microsatellite ((, 2016).

not require any additional components to perform this task.

Space agencies are nowadays building CubeSats larger than the conventional P-POD (Poly-Picosatellite Orbital Deployer) (Puig-Suari et al., 2001) dispense limit, which is 3U. Consequently, a new standard called the *Canisterized Satellite Dispenser (CSD)* has emerged to accommodate larger payloads, including 6U, 12U, and 27U CubeSats (Puig-Suari et al., 2001; Hevnerolemans and Hevner, 2016). CSDs are protective enclosures for CubeSats during launch and facilitate their deployment once in space. These dispensers mitigate the risk of damage to primary payloads or CubeSats housed within them. Addi-

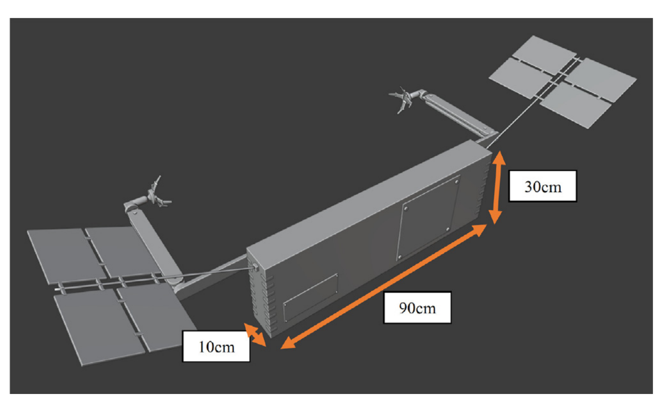

Fig. 7. A 3D model of the designed deorbiter CubeSat.

tionally, the 27U CubeSats can also be deployed using ring deployers like the ESPA (Wegner et al., 2001). In summary, both CSDs and ring deployers offer viable options for dispensing 27U deorbiter CubeSats.

The following sections detail the subsystems of the deorbiter CubeSat, which include vision-based object tracking, robotic arm-based debris capture, and hybrid & active deorbiting strategies employed in this work.

5.1.1. Debris detection and tracking: vision-based object detection & tracking

The tracking system on a satellite is crucial for capturing debris by accurately identifying the target object from the environment and continuously following it. While various sensor-based tracking systems exist, including LiDARs, radar, and cameras, camera-based tracking stands out for its dependable performance, reduced computational demands, seamless integration with onboard computers, cost-effectiveness, and swift sensing capabilities. Therefore, we chose a camera as the sensor system for object tracking. The camera also serves as a feedback sensor to propel the satellite constantly toward the target for precise rendezvous. It identifies and locates the target object in a 3D scene with respect to the deorbiter CubeSat using an advanced deep learning-based object detection technique, and the motion control algorithm directs the camera towards the target object to achieve continuous tracking. The objective of the camera control is to ensure that the satellite in motion is always at the center of the camera image plane, resembling the eye-tracking ability of a human. Fig. 8 shows the camera module used for designing this prototype.

In the prototype, we have used a stereo camera system consisting of two USB-powered 8-megapixel cameras for tracking, which are directly interfaced with a Raspberry Pi, that serves as the central computer to execute vision-based algorithms. The continuous video stream output from the stereo camera system is fed as an input to the object detection and tracking algorithm, running inside the Raspberry Pi.

5.1.1.1. YOLO - object detection framework. The YOLO (You Only Look Once) (Redmon et al., 2016) algorithm is a real-time object detection system that employs a single neural network to simultaneously predict bounding boxes and class probabilities for multiple objects in an image. When applied to video input, YOLO extends its real-time object detection capabilities to sequential frames at more than 60 frames/s. The algorithm divides the input image into a grid and generates bounding boxes within each grid cell, predicting the confidence scores for object presence and the associated class probabilities.

Table 4
Sizes of subsystems in the deorbiter CubeSat.

Subsystem	Size
Spacecraft Avionics & Communication System	**9U**
Vision-based Detection & Tracking Device	**3U**
Dual Robotic Arm-based Capture Device	**9U**
Active Deorbit Device (HET)	**4U**
Passive Deorbit Device (Drag Sail)	**2U**
Overall CubeSat Form Factor	**27U**

In this work, we implemented the YOLOv4-Tiny (Bochkovskiy et al., 2020) on a Raspberry Pi, utilizing the video feed input from a camera to achieve continuous detection and localization of the target object. The YOLOv4-tiny is the compressed version of YOLOv4 designed to train on machines that have less computing power. This framework capitalizes on the advancements in AI and deep learning, resulting in a more efficient and precise object detection and localization system. In this scenario, the model underwent offline training on a computer equipped with a GPU, utilizing a tailored dataset of cardboard box images captured from different angles and distances. The dataset was designed to match the size and dimensions of the XSat. Following training, the model was deployed for detection, achieving a final object detection accuracy of 96.09%, as illustrated in Fig. 9.

Stereo vision computes debris range using dual cameras, while YOLO processes video input for efficient object detection and localization. This integrated approach combines depth perception with accurate identification, enhancing the overall precision of the debris tracking system. The detection range of the lens is critical for ensuring effective object identification and tracking in any optical instrument. The detection range of a camera system R is given by,

$$R = \frac{D \times f}{s}, \tag{3}$$

where D is the size of the debris (diagonal measurement), f is the focal length of the camera, and s is the pixel size on the sensor. The theoretical detection range for the considered vision system can be calculated using the following parameters:

- Given the size of the XSat, which is $60 \times 60 \times 80\ cm^3$, the diagonal size of the CubeSat is, $D = \sqrt{60^2 + 60^2 + 80^2} \approx 116$ cm.
- Focal length of the camera $f = 16$ mm.
- Pixel size $s = 1.26\ \mu$m.

Plugging in these values into Eq. 3, we get $R \approx 1473$ meters ≈ 1.47 km. While the theoretical calculation shows a very high range, practical detection ranges in space are influenced by Relative velocities between the CubeSat and debris, lighting conditions, etc. Given these considerations, the minimum operational detection range for our vision system is typically around 30 to 60 meters (25 to 50 times lower when compared to the theoretical value), which is sufficient for reliable identification and tracking. This range ensures that the debris is detected and accurately classified, considering real-world constraints and the need for precise image processing.

Fig. 8. An 8 MP Camera module interfaced to a Raspberry Pi board.

Adequate illumination is paramount for achieving high-quality image capture and precise detection. In Low Earth Orbit (LEO), sunlight serves as the primary source of illumination. To accommodate diverse lighting conditions such as direct sunlight, shadowed areas, and reflected light from the Earth's surface or debris, the cameras and sensors are outfitted with filters and adaptive exposure controls. In instances where consistent lighting is essential, particularly during eclipse periods, low-power LED illumination can be integrated.

In this work, we assume that the deorbit spacecraft is deployed into a matching orbit with the XSat so that trajectory corrections and rendezvous take minimal fuel. Upon identifying the target debris object, the Hall-effect thrusters, assisted by the stereo vision camera system, execute a precise rendezvous. This is achieved using the range information and the object's position within the camera frame.

The next section details the debris capture subsystem.

5.1.2. Debris capture: dual robotic arms

Over the past 50 years, robots have significantly replaced humans in tightly controlled environments, such as goods packaging, vehicle assembly lines, handling hazardous materials, welding and painting metal parts, picking and placing heavy objects, and more. Among the various applications of robots, capture tasks require robotic arms, which are attached to fixed or mobile platforms. Robotic arm-based capture involves one or more robotic arms controlled and coordinated to grasp an object of interest using real-time sensor feedback on the object's position relative to the arm's coordinates. Industrial arms typically weigh more than 100 kg and are large. However, for satellite applications, especially on CubeSats, the size and weight of the arm system are critical factors. Therefore, for this prototype, we have chosen a pair of robotic arms to perform debris capture.

Fig. 9. Detection accuracy of 96.09% obtained by the vision-based tracking system.

As shown in Fig. 10, two retractable robotic arms with 4 degrees of freedom (DoF), each 40 cm in length are mounted to the sides of the CubeSat. When the CubeSat is not performing debris capture, the arms are folded into a smaller form factor and stowed inside the lateral surfaces on either side of the CubeSat. The four identical revolute joints of the arm provide 4 degrees of freedom to the arms. For the grasping task, this selected kinematic structure is redundant, allowing for higher arm dexterity and robustness to singularities. Each robotic arm is controlled using 4 servo motors and a total of 8 motors are being used to construct the prototype of the capture subsystem.

Besides designing a mechanical system for capture, it is equally important to grasp the target object smoothly, to prevent additional debris from being created due to mishandling. So, to achieve smoother yet tight capture, we have designed a pair of soft robotic gripping claws using silicon rubber, which is pneumatically controlled and activated by range sensors, to perform precise capture. Each claw is attached to the robotic arm as shown in Fig. 11.

To ensure accurate debris capture, arm motion for both arms must be coordinated. This has been achieved by programming the servo controllers to operate in a 180° out-of-phase motion for both arms, in a time-synchronous manner. This ensures the simultaneous engagement of both arms for a perfect capture. The set of coordinated moves for the two arms for debris capture is illustrated in Fig. 12. Upon triggering the control input, both the arms are engaged in tandem and tightly grasp the XSat using their soft claws from either side for deorbiting. Fig. 13 depicts the intended debris capture. A short video demonstration of the same can be viewed by visiting https://www.youtube.com/watch?v=6UNDeGEenJA.

Once the debris object is captured successfully, the deorbit mechanism is initialized for debris removal, which the next section describes in detail.

5.1.3. Electrical Power System (EPS)

One of the core subsystems on any satellite is the electrical power system, called EPS. The function of the EPS is to provide stable input power to all the subsystems. Solar panels mounted onto the sides and the surface of the CubeSat convert the light energy from the Sun into electrical

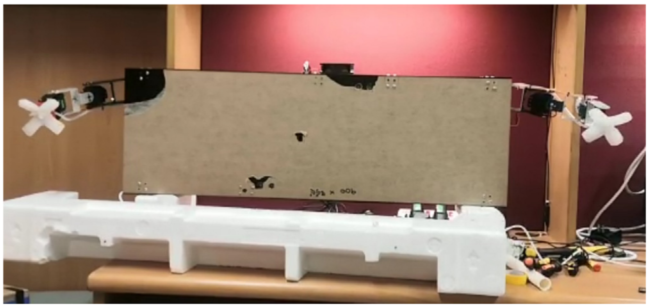

Fig. 10. CubeSat prototype with dual robotic arms.

energy during each non-eclipse phase and store that energy inside the onboard lithium polymer batteries. From the power budget requirements, we have concluded that 8 solar panels are necessary to generate the necessary energy for the uninterrupted deorbiter operation. A maximum power point tracking (MPPT) device is equipped on board to maximize power extraction through the regulated orientation of the solar panel. A parallel connection is made between the battery and the buck-boost converter, which steps up the 3.7 V input to a 5 V output voltage, and feeds it to all the CubeSat subsystems.

5.1.4. Debris deorbit mechanisms: hybrid & active deorbiting

Spacecraft that are launched at altitudes less than 450 km naturally decay in well under 25 years. However, at orbit altitudes beyond 550 km, it can no longer be guaranteed due to uncertainties in atmospheric density and other environmental parameters. As additional propellant is required to transfer these satellites to a higher graveyard orbit, the only viable option for spacecraft in lower orbits is to deorbit into the Earth's atmosphere.

As the XSat is orbiting the Earth at 817 km orbit, passive deorbit techniques alone would not be sufficient. So, in this work we explore an active deorbit technique, using two Hall-effect thrusters. The redundant thruster can be used for precise rendezvous and to control the satellite attitude. For the second deorbit scenario, we present a hybrid deorbit mechanism, in which the orbit lowering is performed using the active deorbiting technique, and the entry into the atmosphere is performed using a passive deorbit technique. In a hybrid deorbiting scheme, the satellite is brought down to 500 km altitude using the Hall-effect thruster and a drag sail deorbits the satellite from there. This would result in a mission design with lesser fuel requirement, at the cost of higher deorbit times.

The later sections analyze these two deorbit mechanisms in detail.

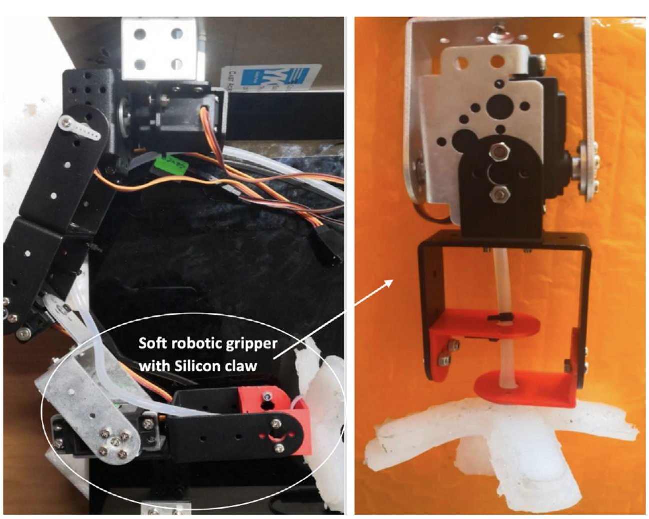

Fig. 11. Stowed robotic arm with a silicon claw.

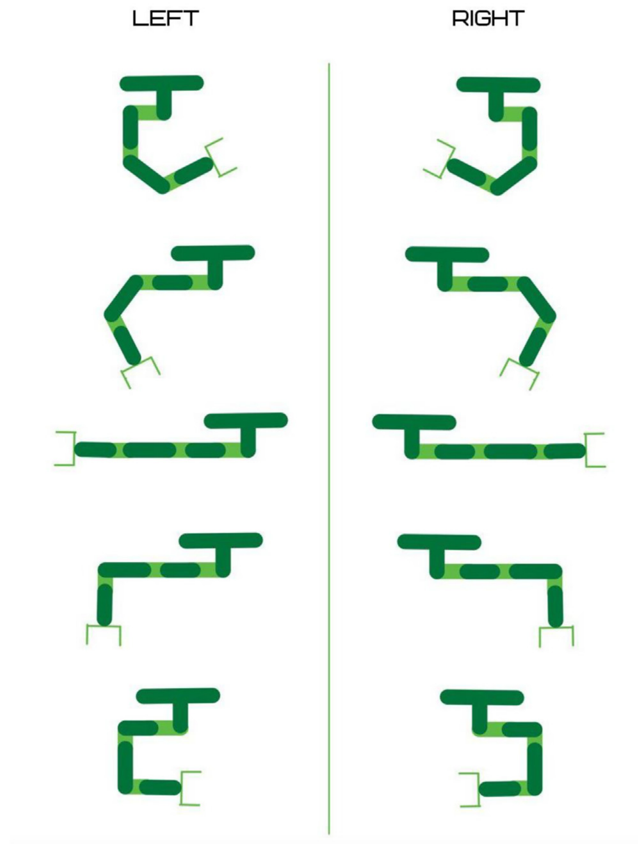

Fig. 12. Coordinated motion control of the robotic arms.

5.2. Delta-V computation for active deorbiting

The change in velocity, often referred to as *delta-V*, is the most important measure of the transfer cost. A delta-v budget is an estimate of *the total change in velocity required for a space mission*. It is often calculated as the sum of the delta-v required to perform each propulsive maneuver needed during the mission. In this work, during the active deorbit phase, multiple tangential burns are performed by firing the Hall-effect thrusters during each orbit, resulting in a spiral trajectory towards the Earth to achieve the desired orbital decay. Simulations for the delta-V cost computation have been carried out using the Systems Tool Kit (STK) Astrogator, a high-fidelity orbit propagator tool

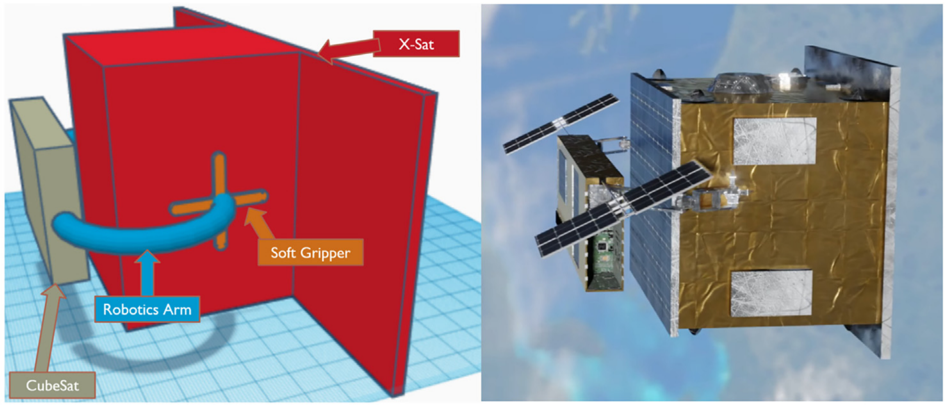

Fig. 13. Intended XSat Capture.

developed by Analytical Graphics, Inc. (AGI, 2021). The delta-V that is required to deorbit the XSat from its current orbit to lower altitudes, i.e. to a 500 km orbit for passive deorbiting is **160 m/s** and to a 350 km orbit for complete active deorbiting is **240 m/s**.

For the two deorbit methods, the analysis of required propellant mass and orbital decay are presented next.

5.3. Passive deorbiting: effects of drag surface area on orbital decay

The hybrid deorbit scheme of the XSat deorbit mission contains two phases, (1) active deorbiting of the satellite to 500 km altitude, and (2) deorbiting it from there using a passive deorbit device. The performance of passive deorbit techniques relies heavily on the variation of environmental parameters, such as the atmospheric density, solar flux F 10.7 cm, geomagnetic indices, etc., and also on the deorbit device-specific parameters such as the drag surface area, etc. In this section, we present the simulation results obtained for the orbital decay of the deorbiting CubeSat for various drag surface area increments deorbiting from 500 km altitude. The drag coefficient of the surface is considered as 2.2 throughout the orbital decay analysis. Fig. 14 illustrates the effect of the surface area increment on the CubeSat deorbiter lifetime. It is clear from the plot that the satellite lifetime (deorbiting the debris) will be greatly reduced through a careful increment of the drag surface area.

5.4. Active and hybrid deorbiting: propellant mass requirement for XSat Deorbit Mission

The fundamental idea behind active deorbiting for space debris is to use retrograde propulsion to accelerate the orbital decay. In our CubeSat design, two Hall-effect thrusters are employed for satellite propulsion. We assume that the capacity of the battery pack is 133.2 Wh with 25% depth of discharge, and the solar panels contain 96 solar cells, which ensure a full battery recharge in one orbit, during its traversal on the sun side. This would ensure peak performance for the two 50 W input power, 800s specific impulse Hall-effect thrusters operated during the eclipse phase. The mass of the 27U CubeSat deorbiter is approximately 25 kg and the XSat is 106 kg. Hence, the total dry mass of the deorbiter CubeSat is **131 kg**. The mass of the propellant m_p required to deorbit a satellite of total mass m_t is given by

$$m_p = m_t(1 - \exp(-\Delta V / g_0 I_{sp})), \quad (4)$$

where I_{sp} is the specific impulse of the Hall-effect thruster, g_0 is the standard gravitational acceleration and ΔV is the required change in velocity.

Fig. 15 depicts the variation in deorbit time to actively deorbit XSat from 817 km orbit to lower altitudes in LEO, to 500 km and 350 km in this case. The x-axis of the plot represents the deorbit time in days, and the y-axis of the plot indicates the orbit altitude in km.

Using Eq. 4, the required propellant mass for this deorbit mission can be computed. The total orbital decay time for the active and hybrid deorbit schemes is computed from the total thruster burn time to achieve the desired ΔV. These values are illustrated in Table 5. From Table 5 we can conclude that a drag sail of 4 m^2 cross-sectional area would significantly reduce the debris lifetime and deorbits the XSat within 2.81 years.

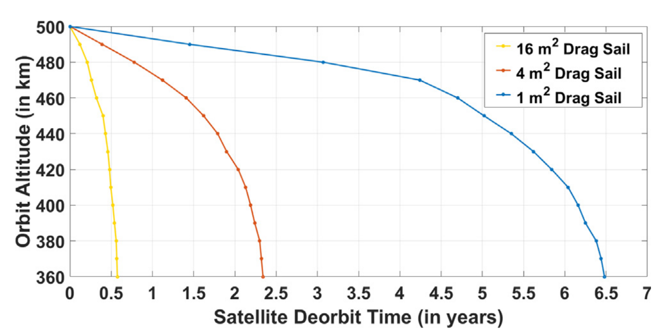

Fig. 14. Orbital decay of the XSat deorbiter CubeSat from 500 km altitude for variable drag surface area.

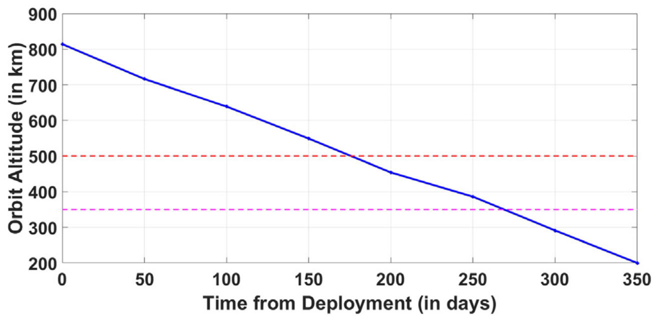

Fig. 15. Orbital decay for the XSat deorbiter CubeSat from 817 km altitude using active deorbit mechanism.

Table 5
Comparison of the active and hybrid deorbit mechanisms.

Deorbit Technique	Deorbit Time(in years)	Propellant Mass(in kg)
Active	**0.75**	**19.3**
Hybrid (1 m^2 Sail)	**6.99**	**12.7**
Hybrid (4 m^2 Sail)	**2.81**	**12.7**

6. Discussion

In this study, we examined the efficiency of a CubeSat-based system and its effectiveness in servicing debris at various altitudes. To design a space mission within a reasonable budget, CubeSats larger than 27U become economically unfeasible due to high launch and development costs. Additionally, in determining the upper limit on debris mass, particularly at lower altitudes (below 500 km), the mass of the CubeSat becomes insignificant when compared to the debris mass ($m_d \gg m_s$ or $m_d \approx m_d + m_s$). The upper limit on debris mass increases with the drag cross-sectional area at a given orbit altitude for a fixed CubeSat form factor.

For a deorbiter CubeSat sized at 6U, where the avionics and communication devices occupy a 3U form factor, leaving only 3U for the deorbit payload, the 6U form factor may not be a practical deorbit platform. Similarly, a 12U CubeSat, with an available 9U form factor for debris removal payloads, might struggle to accommodate the necessary tracking, rendezvous, capture, and deorbit devices due to limited space. Moreover, the upper limit on debris mass that the 6U and 12U CubeSats can deorbit from orbits below 550 km is less than 100 kg. Therefore, a CubeSat with a 27U form factor is necessary for deorbiting defunct satellites with masses above 100 kg, such as the XSat. Additionally, considering fuel consumption, the hybrid deorbit technique (combining active and passive methods) could be a potential candidate for orbital debris deorbit missions due to its economic viability. Increasing the drag cross-sectional area would significantly reduce the satellite's lifetime, ensuring faster orbital decay.

7. Conclusions

This paper presents a comprehensive system-level study on orbital debris removal from LEO, covering the debris removal process and various tracking, rendezvous, capture, and deorbit mechanisms. It identifies CubeSat-compatible capture and deorbit mechanisms as economical and reusable solutions for LEO debris removal. The upper bound on debris mass deorbited from distinct LEO altitudes using CubeSats of different form factors is computed. A design for the deorbiter CubeSat, integrating selected mechanisms, is proposed, along with a detailed prototype of a dual robotic arm-based debris capture subsystem. An object detection algorithm based on deep learning enhances debris detection and localization accuracy. Additionally, delta-V and propellant mass for Hall-effect thrusters in the active deorbiting scenario are computed, and a lifetime analysis of the deorbiting XSat, considering drag surface area impact, is conducted.

CubeSats are primarily suitable for deorbiting other CubeSats or microsatellites under 50 kg mass at lower altitudes due to payload volume limitations. Form factors like 6U and 12U are typically restricted to this capacity, effective below 500 km altitude. However, larger form factors, like 27U, are necessary to deorbit larger satellites such as XSat and those at higher altitudes. Without active deorbiting, XSat's estimated orbit lifetime exceeds 500 years, which can be reduced to 7 years or less using hybrid deorbiting techniques by increasing the satellite's drag surface area. Analysis shows the feasibility of a CubeSat design for XSat deorbiting. A preliminary prototype of the deorbiter CubeSat exists, with ongoing efforts to enhance it for laboratory testing. Future work includes detailed mission design for XSat deorbiting.

Declaration of Competing Interest

The authors declare that they have no known competing financial interests or personal relationships that could have appeared to influence the work reported in this paper.

Acknowledgments

This work was supported by the National Research Foundation (NRF), Singapore under the Intra-CREATE agreement NRF2018-ITS004-0008.

Appendix A. Supplementary material

Supplementary data associated with this article can be found, in the online version, at https://doi.org/10.1016/j.asr.2024.08.009.

References

AGI, 2021. System Tool Kit (STK). https://www.agi.com/products/stk.

Aglietti, G.S., Taylor, B., Fellowes, S., Salmon, T., Retat, I., Hall, A., Chabot, T., Pisseloup, A., Cox, C., Mafficini, A., et al., 2020. The active space debris removal mission RemoveDebris. Part 2: in orbit operations. Acta Astronaut. 168, 310–322. https://doi.org/10.1016/j.actaastro.2019.09.001.

Astroscale, 2019. Astroscale. https://astroscale.com/about-astroscale/about/.

Barbee, B.W., Alfano, S., Pinon, E., Gold, K., Gaylor, D., 2011. Design of spacecraft missions to remove multiple orbital debris objects. In: In 2011 Aerospace Conference. IEEE, pp. 1–14. https://doi.org/10.1109/AERO.2011.5747303.

Bérend, N., Olive, X., 2016. Bi-objective optimization of a multiple-target active debris removal mission. Acta Astronaut. 122, 324–335. https://doi.org/10.1016/j.actaastro.2016.02.005.

Bochkovskiy, A., Wang, C.-Y., & Liao, H.-Y.M. (2020). Yolov4: Optimal speed and accuracy of object detection. arXiv preprint arXiv:2004.10934, https://doi.org/10.48550/arXiv.2004.10934.

Bonnal, C., Ruault, J.-M., Desjean, M.-C., 2013. Active debris removal: Recent progress and current trends. Acta Astronaut. 85, 51–60. https://doi.org/10.1016/j.actaastro.2012.11.009.

Braun, V., Lüpken, A., Flegel, S., Gelhaus, J., Möckel, M., Kebschull, C., Wiedemann, C., Vörsmann, P., 2013. Active debris removal of multiple priority targets. Adv. Space Res. 51 (9), 1638–1648. https://doi.org/10.1016/j.asr.2012.12.003.

Bylard, A., MacPherson, R., Hockman, B., Cutkosky, M.R., Pavone, M., 2017. Robust capture and deorbit of rocket body debris using controllable dry adhesion. In: 2017 IEEE Aerospace Conference. IEEE, pp. 1–9. https://doi.org/10.1109/AERO.2017.7943844.

CalPoly (2014). Cubesat design specification, rev. 13. The CubeSat Program, California Polytechnic State University, Cal Poly SLO,.

Cerf, M., 2015. Multiple space debris collecting mission: optimal mission planning. J. Optim. Theory Appl. 167 (1), 195–218. https://doi.org/10.1007/s10957-015-0705-0.

Chandra, A., Wilburn, G., Thangavelautham, J., 2019. Advanced inflatable de-orbit solutions for derelict satellites and orbital debris. In: 2019 Space Traffic Management Conference.

CleanSpaceOne (2019). The CleanSpace One. https://www.cleanspace-one.ch/.

DeLuca, L., Bernelli, F., Maggi, F., Tadini, P., Pardini, C., Anselmo, L., Grassi, M., Pavarin, D., Francesconi, A., Branz, F., et al., 2013. Active space debris removal by a hybrid propulsion module. Acta Astronaut. 91, 20–33. https://doi.org/10.1016/j.actaastro.2013.04.025.

EOPortal (2016). X-Sat of NTU (Nanyang Technological University), Singapore. https://directory.eoportal.org/web/eoportal/satellite-missions/v-w-x-y-z/xsat.

ESA (2016). Active Debris Removal. https://www.esa.int/Safety_Security/Space_Debris/Active_debris_removal.

ESA (2019). ESA spacecraft dodges large constellation. https://www.esa.int/Safety_Security/ESA_spacecraft_dodges_large_constellation.

ESA (2023). Space environment statistics. https://sdup.esoc.esa.int/discosweb/statistics/.

ESOC (2023). ESA's Annual Space Environment Report, ESOC. https://www.sdo.esoc.esa.int/environment_report/Space_Environment_Report_latest.pdf.

Felicetti, L., Gasbarri, P., Pisculli, A., Sabatini, M., Palmerini, G.B., 2016. Design of robotic manipulators for orbit removal of spent launchers' stages. Acta Astronaut. 119, 118–130. https://doi.org/10.1016/j.actaastro.2015.11.012.

Feng, L.W.-Y., Martinez, P., Dropmann, M., Ehresmann, M., Ginsberg, S., Herdrich, G., Laufer, R., 2017. MEDUSA–mechanism for entrapment of debris using shape memory alloy. In: 67th International Astronautical Congress (pp. 01–02).

Fernandez, J., Schenk, M., Prassinos, G., Lappas, V., Erb, S., 2013. Deployment mechanisms of a gossamer satellite deorbiter. In: 15th European Space Mechanisms and Tribology Symposium, Noordwijk, The Netherlands.

Forshaw, J.L., Aglietti, G.S., Fellowes, S., Salmon, T., Retat, I., Hall, A., Chabot, T., Pisseloup, A., Tye, D., Bernal, C., et al., 2020. The active space debris removal mission RemoveDebris. Part 1: from concept to launch. Acta Astronaut. 168, 293–309. https://doi.org/10.1016/j.actaastro.2019.09.002.

Gaposchkin, E.M., Coster, A.J., 1988. Analysis of satellite drag. Lincoln Lab. J. 1, 203–224.

Guglielmo, D., Omar, S., Bevilacqua, R., Fineberg, L., Treptow, J., Poffenberger, B., Johnson, Y., 2019. Drag deorbit device: a new standard reentry actuator for cubesats. J. Spacecr. Rock. 56 (1), 129–145. https://doi.org/10.2514/1.A34218.

Hakima, H., Bazzocchi, M.C., Emami, M.R., 2018. A deorbiter cubesat for active orbital debris removal. Adv. Space Res. 61 (9), 2377–2392. https://doi.org/10.1016/j.asr.2018.02.021.

Hakima, H., Emami, M.R., 2018. Assessment of active methods for removal of LEO debris. Acta Astronaut. 144, 225–243. https://doi.org/10.1016/j.actaastro.2017.12.036.

Holemans, W., Hevner, R., 2016. Canisterized satellite dispenser. US Patent 9,415,883.

Kan, S., 2007. China's anti-satellite weapon test. Congressional Research Service (Library of Congress, Washington DC).

Kyushu, 2020. Designing and Developing the World's First Satellite for Removing Space Debris with a Laser. https://www.kyushu-u.ac.jp/en/notices/view/196.

Lappas, V., Adeli, N., Visagie, L., Fernandez, J., Theodorou, T., Steyn, W., Perren, M., 2011. Cubesail: A low cost cubesat based solar sail demonstration mission. Adv. Space Res. 48 (11), 1890–1901. https://doi.org/10.1016/j.asr.2011.05.033.

Liou, J.-C., 2006. Collision activities in the future orbital debris environment. Adv. Space Res. 38 (9), 2102–2106. https://doi.org/10.1016/j.asr.2005.06.021.

Liou, J.-C., 2013. Engineering and technology challenges for active debris removal. Prog. Propul. Phys. 4, 735–748. https://doi.org/10.1051/eucass/201304735.

Liou, J.-C., 2014. Modeling the large and small orbital debris populations for environment remediation. In: Third European Workshop on Space Debris Modeling and Environment Remediation, CNES HQ, Paris, France, pp. 16–18.

Liou, J.-C., 2018. Overview of the orbital debris environment. In: 2018 Space Traffic Management Conference.

Liou, J.-C., Johnson, N.L., 2006. Risks in space from orbiting debris. Science 311 (5759), 340–341. https://doi.org/10.1126/science.1121337.

Liou, J.-C., Johnson, N.L., Hill, N., 2010. Controlling the growth of future LEO debris populations with active debris removal. Acta Astronaut. 66 (5–6), 648–653. https://doi.org/10.1016/j.actaastro.2009.08.005.

Liou, J.-C., Shoots, D., 2009. Satellite collision leaves significant debris clouds. Orbital Debris Q News 13 (2), 1.

Lucken, R., Hubert, N., Giolito, D., 2017. Systematic space debris collection using cubesat constellation. In: Proceedings of the 7th European Conference for Aeronautics and Aerospace Sciences (EUCASS), Milan, Italy (pp. 3–6). https://doi.org/10.13009/EUCASS2017-678.

Mark, C.P., Kamath, S., 2019. Review of active space debris removal methods. Space Policy 47, 194–206. https://doi.org/10.1016/j.spacepol.2018.12.005.

Missel, J., Mortari, D., 2013. Removing space debris through sequential captures and ejections. J. Guidance, Control, Dynam. 36 (3), 743–752. https://doi.org/10.2514/1.58768.

MITTechnologyReview, 2011. A Sticky Solution for Grabbing Objects in Space. https://www.technologyreview.com/2011/10/05/190896/a-sticky-solution-for-grabbing-objects-in-space/.

Morin, J., 2019. Four steps to global management of space traffic. Nature 567, 25–27. https://doi.org/10.1038/d41586-019-00732-7.

NASA, 2017. Space Debris and Human Spacecraft https://www.nasa.gov/mission_pages/station/news/orbital_debris.html.

Nishida, S.-I., Kawamoto, S., 2011. Strategy for capturing of a tumbling space debris. Acta Astronaut. 68 (1–2), 113–120. https://doi.org/10.1016/j.actaastro.2010.06.045.

NOAA, 2020. F10.7cm radio emissions. https://www.swpc.noaa.gov/phenomena/f107-cm-radio-emissions.

Nock, K., Gates, K., Aaron, K., McRonald, A., 2010. Gossamer orbit lowering device (GOLD) for safe and efficient de-orbit. In: AIAA/AAS Astrodynamics specialist conference (p. 7824). doi: 10.2514/6.2010-7824.

Phipps, C.R., Bonnal, C., 2016. A spaceborne, pulsed UV laser system for re-entering or nudging LEO debris, and re-orbiting GEO debris. Acta Astronaut. 118, 224–236. https://doi.org/10.1016/j.actaastro.2015.10.005.

Picone, J., Hedin, A., Drob, D.P., Aikin, A., 2002. NRLMSISE-00 empirical model of the atmosphere: Statistical comparisons and scientific issues. J. Geophys. Res.: Space Phys. 107 (A12), SIA-15. https://doi.org/10.1029/2002JA009430.

Puig-Suari, J., Turner, C., Ahlgren, W., 2001. Development of the standard cubesat deployer and a cubesat class picosatellite. In: 2001 IEEE aerospace conference proceedings (cat. No. 01TH8542) (pp. 1–347). IEEE volume 1. doi: 10.1109/AERO.2001.931726.

Redmon, J., Divvala, S., Girshick, R., Farhadi, A., 2016. You only look once: Unified, real-time object detection. In: Proceedings of the IEEE conference on computer vision and pattern recognition (pp. 779–788). doi: 10.1109/CVPR.2016.91.

Romagnoli, D., Theil, S., 2012. De-orbiting satellites in LEO using solar sails. J. Aerospace Eng., Sci. Appl. 4 (2), 49.

Shan, M., Guo, J., Gill, E., 2016. Review and comparison of active space debris capturing and removal methods. Prog. Aerosp. Sci. 80, 18–32. https://doi.org/10.1016/j.paerosci.2015.11.001.

Shan, M., Guo, J., Gill, E., 2017. Deployment dynamics of tethered-net for space debris removal. Acta Astronaut. 132, 293–302. https://doi.org/10.1016/j.actaastro.2017.01.001.

Shen, H.-X., Zhang, T.-J., Casalino, L., Pastrone, D., 2018. Optimization of active debris removal missions with multiple targets. J. Spacecr. Rock. 55 (1), 181–189. https://doi.org/10.2514/1.A33883.

Takahashi, K., Charles, C., Boswell, R.W., Ando, A., 2018. Demonstrating a new technology for space debris removal using a bi-directional plasma thruster. Scient. Rep. 8 (1), 14417. https://doi.org/10.1038/s41598-018-32697-4.

Tapping, K., 2013. The 10.7 cm solar radio flux (F10. 7). Space Weather 11 (7), 394–406. https://doi.org/10.1002/swe.20064.

Trentlage, C., Stoll, E., 2015. The applicability of gecko adhesives in a docking mechanism for active debris removal missions. In: 13th Symposium on Advanced Space Technologies in Robotics and Automation, ASTRA.

Wegner, P.M., Ganley, J., Maly, J.R., 2001. EELV secondary payload adapter (ESPA): providing increased access to space. In: 2001 IEEE Aerospace Conference Proceedings (Cat. No. 01TH8542) (pp. 2563–2568). IEEE volume 5. doi: 10.1109/AERO.2001.931218.

Wilde, M., Walker, I., Kwok Choon, S., Near, J., 2017. Using tentacle robots for capturing non-cooperative space debris-A proof of concept. In: AIAA SPACE and Astronautics Forum and Exposition (p. 5246). doi: 10.2514/6.2017-5246.

Witze, A., 2019. SpaceX launch highlights threat to astronomy from 'megaconstellations'. Nature 575 (7782), 268–270. https://doi.org/10.1038/d41586-019-03446-y.

Yamamoto, T., Murakami, N., Nakajima, Y., Yamanaka, K., 2014. Navigation and trajectory design for Japanese active debris removal mission. In: 24th International Symposium on Space Flight Dynamics. Johns Hopkins University Applied Physics Laboratory Laurel, Maryland, USA, pp. 1–29.

Yu, J., Chen, X.-Q., Chen, L.-H., 2015. Optimal planning of LEO active debris removal based on hybrid optimal control theory. Adv. Space Res. 55 (11), 2628–2640. https://doi.org/10.1016/j.asr.2015.02.026.